J. Phys. G: Nucl. Phys. **14** (1988) 1125–1137. Printed in the UK

Fragmentation of ^{22}Ne in emulsion at 4.1*A* GeV/*c*

A El-Naghy[1]†, S A Krasnov[1], K D Tolstov[1], N P Andreeva[2], Z V Anzon[2], V I Bubnov[2], I Ya Chasnikov[2], G Zh Eligbaeva[2], L E Eremenko[2], A Sh Gaitinov[2], G S Kalyachkina[2], E K Kanygina[2], Ts I Shakhova[2], M Gitsok[3], M Haiduc[3], V Topor[3], V A Leskin[4], J A Salomov[5], F G Lepekhin[6], B B Simonov[6], M Karabova[7], M Totova[7], S Vokal[7], E Siles[7], V A Antonchik[8], S G Bogdanov[8], A Y Likhachev[8], V I Ostroumov[8], V G Bogdanov[9], V A Plyushchev[9], Z I Solovieva[9], M I Adamovich[10], M M Chernyavski[10], S P Kharlamov[10], V G Larionova[10], N V Maslennikova[10], G I Orlova[10], N A Salmanova[10], M I Tretyakova[10], A V Belousov[11], M Sumbera[12], N I Kostanashvili[13], L Sardamba[14], R Togoo[14], D Tuvdendorzh[14], F A Avetyan[15], V M Krishchyan[15], M A Marutyan[15], L G Sarkisova[15] and V R Sarkisyan[15]

[1] Joint Institute for Nuclear Research, Dubna, USSR
[2] Institute of High Energy Physics, Alma-Ata, USSR
[3] Central Institute of Physics, Bucharest, Romania
[4] Physical Technical Institute of Dushanbe, USSR
[5] Tadjik State University, Dushanbe, USSR
[6] Leningrad Nuclear Physical Institute, Gatchina, USSR
[7] Safarik University, Kosice, Czechoslovakia
[8] Leningrad Polytechnic Institute, Leningrad, USSR
[9] V G Khlopin Radium Institute, Leningrad, USSR
[10] P N Lebedev Physical Institute, Moscow, USSR
[11] Azovo-Chernomorski Institute of Agriculture Mechanization, Rostov on Don, USSR
[12] Nuclear Physics Institute, Řež, Czechoslovakia
[13] Tbilisi State University, Tbilisi, USSR
[14] Institute of Physics and Technology, Ulan-Bator, Mongolia
[15] Yerevan Physical Institute, Yerevan, USSR

Received 19 August 1987, in final form 9 March 1988

Abstract. Charge distributions of projectile fragments produced in the interactions of ^{22}Ne beams with emulsion at 4.1*A* GeV/*c* have been studied. Correlations between projectile and target fragments and among projectile fragments are presented. The change of charge yield distribution with the violence of the collision has been shown. The present analysis contradicts theoretical calculations describing the inclusive charge yield distribution of fragments by a single process.

1. Introduction

In nucleus–nucleus collisions, the nucleons in the overlap region are called participants. The remaining nucleons are spectators. Large impact parameters lead to 'gentle' reactions while small ones give 'violent' interactions. The spectators are the prefragments which decay further into fragments. The mechanism of this process is still a matter of debate. Fragmentation is one of the historical [1] and fundamental

† On leave of absence from Cairo University, Cairo, Egypt.

0305-4616/88/081125 + 13 $02.50

questions [2–4] in high-energy nuclear physics. The author of [2] schematically distinguished three main mechanisms for the fragmentation of $A \geqslant 200$ prefragment nuclei: the first is spallation, which leads to one fragment of mass near to that of the prefragment nucleus; the second is fission, which gives two heavy fragments, each of mass close to half the prefragment nucleus mass; and the third is multifragmentation, which provides several fragments. In [3, 4] the fragmentation processes are divided according to the temperature, T, of the prefragment nucleus as follows: at $T \leqslant 5$ MeV the mass yield distribution is localised near the minimal and maximal masses corresponding to single nucleons and residual nuclei. At $T \simeq 5$–7 MeV the mass distribution has a U-shaped form which indicates the multifragmentation threshold. At $T > 7$ the inclusive mass yield distribution becomes a monotonic decreasing function, the steepness of which increases with increasing T.

Many theoretical models have been devoted to the study of the multifragmentation process [2–16]. In some models, the prefragment nucleus heats up and then condenses into droplets [5, 6]. In others, it simply evaporates the fragments sequentially [7]. In [8–13], the fragments are statistically emitted from an intermediate excited nuclear system. Other statistical approaches [14–16] try to explain multifragmentation without any reference to thermal equilibrium, i.e. as shattering of the prefragment nucleus into many pieces. A detailed description of different multifragmentation models is given in the review articles [2–4].

To study the multifragmentation mechanism, a huge number of experiments have been carried out. These experiments dealt with heavy-target-nucleus fragmentation induced by energetic protons and ions (e.g., [17, 18]). The use of heavy-ion beams has an important experimental advantage: one can study the fragments produced by the disintegration of the projectile nucleus. The fragments of the projectile nucleus are fast, distinguishable and can be easily measured in detectors and/or spectrometers while the target fragments are slow, difficult to measure and often stop in the target material. Most of the heavy-target fragmentation experiments gave one-particle inclusive measurements, e.g. the charge $d\sigma/dZ$ or mass $d\sigma/dA$ yield of the fragments. Various models predicted nearly the same form of $d\sigma/dZ$ and $d\sigma/dA$. Thus these data turned out to be inconclusive with respect to various models.

In the present experiment all projectile fragments (PF) were recorded, and their charges and emission angles were measured. Thus we have exclusive data which enable one to study different types of fragment distributions, correlations and comparison with theoretical models. It is of particular interest to test whether fragments are emitted from one source at a single excitation energy.

In the present study, two samples of 4.1A GeV/c ^{22}Ne–emulsion collisions have been used. The first sample consists of 4307 events measured in this experiment (EXP) and the second consists of 4976 events simulated in a computer by the cascade-evaporation model (CEM) [19] under the same experimental conditions.

The paper is organised so that §2 presents the physical implications of the used code of the CEM. The details of the experiment are described in §3. Section 4 provides the selection criteria for the studied events. The results and discussions are outlined in §5. Section 6 is devoted to the conclusions of the paper.

2. Model and scheme of calculations

The proposed model is a development of the intranuclear cascade code [20], used for the description of hadron–nucleus interactions, to the case of nucleus–nucleus colli-

sions at high energies. Each of the colliding nuclei, in its reference frame, is treated as a Fermi gas of nucleons in a potential well $V(r) = B + P_F^2/2m$, where m is the mass of a free nucleon and B is the average binding energy of a nucleon inside a nucleus, which is nearly equal to 7 MeV. Nucleons have a momentum distribution inside a nucleus of the form $W(P)\,dP \simeq P^2\,dP$, $0 \leqslant P \leqslant P_F(r)$ which is isotropic in momentum space. The maximum value of the local Fermi momentum $P_F(r)$ can be expressed in terms of the nuclear density $\rho(r)$, $P_F = \hbar[3\pi^2\rho(r)]^{1/3}$. In practice, this distribution is cut off at a distance R, where $\rho(R)/\rho(0) = 0.01$. The form of the nuclear density is an oscillatory one for nuclei with mass number $A \leqslant 16$ and a Wood–Saxon one for $A > 16$. The distance between any two of the A nucleons in a nucleus is taken to be not less than $2r_c$, where $r_c = 0.4$ fm which is the radius of a nucleon core.

A nucleon of the incident nucleus, in the laboratory system, is considered to be an independent particle which is characterised by a 4-vector of spacetime $[\boldsymbol{r}, t]$, a 4-vector of momentum–energy $[\boldsymbol{P}, E]$ and of effective mass $m_{\text{eff}} = (E^2 - P^2)^{1/2} = m - V(r)$. This consideration is also valid for a target nucleus nucleon in a reference frame connected with the incident nucleus. The effect of the nuclear potential on a particle entering the nucleus is taken into consideration through the sudden approximation, by increasing the particle kinetic energy by the quantity $V(r)$.

Introducing the approximation of an independent particle with an effective mass allows one to use relativistic kinematics, taking into consideration the effect of relativistic compression and the symmetry of the problem relative to the colliding nuclei. In fact, this is one of the basic assumptions of the model which turns the interaction of two complex systems into the interaction between their constituents. Since nuclei move with relativistic velocity, the suggestions made are not obvious and they can be fulfilled only *a posteriori*.

The dynamics of the interaction are followed in time by using the Monte Carlo method. The model takes into consideration the interaction between the nucleons of the two colliding nuclei and those of the cascading particles with nucleons of both nuclei. The collisions between the cascading particles and themselves are neglected. As is usually accepted in the intranuclear cascade models, a fast incident particle can interact with any target nucleon located in its path with a cylindrical cut of cross sectional area $\pi(r_{\text{int}} + \lambda_D)^2$, where λ_D is the de Broglie wavelength and r_{int} is a quantity which is nearly double the value of the strong interaction range and is taken to be 1.3 fm[20]. Thus the probability of scattering on the Kth nucleon after traversing without interaction $(K-1)$ nucleons is given by the binomial distribution:

$$\omega_K = \sum_{i=1}^{K-1} (1 - q_i) q_K.$$

The partial probability q_i $(i = 1, 2, \ldots, k-1)$ is expressed in terms of the interaction cross section on the ith nucleon, σ_i, $q_i = \sigma_i/(r_{\text{int}} + \lambda_D)^2$.

Tracing the time evolution of the interacting system, at a fixed time t all possible collisions are considered and we choose the one which is realised before the others, i.e. $\Delta t = \min(t_i)$, and the system is moved towards a new moment $t \to t + \Delta t$. Thus, for two-particle collisions chosen in this way, the reaction characteristics are selected at random and the obeying of the Pauli exclusion principle is checked. In the case of collision of nucleons from the two colliding nuclei, the Pauli principle is checked in the rest system of the target nucleus as well as in that of the projectile.

In the case of hadron–nucleon collisions, the process of meson formation is

considered as in the usual cascade calculations [20].

It is worthwhile mentioning that the nuclear nucleon, with which an interaction has occurred, is considered as a cascade particle in the further steps and is no longer a constituent of the nuclear system. This causes local change of the nuclear density (the trailing effect [20, 21]) in collisions of two nuclei.

The cascading stage ends when the interacting nuclei are separated by a distance such that their potential wells do not overlap further and all cascading particles are emitted from the nuclei or absorbed by them. As usual in cascade calculation [20], particles inside the nucleus are followed to a certain minimum kinetic energy $V(R)+T_{cut}$. A particle with energy less than the minimum value is absorbed by the nucleus. According to [20], T_{cut} equals $V_{Coul}(R)$ for π mesons and $T_{cut}=V_{Coul}+B$ for nucleons, where $V_{Coul}(R)$ is the Coulomb potential energy on the outer boundary of the nucleus. The estimation of the number of residual nucleons in the potential well and their isotopic constitution gives the mass and charge numbers of the residual excited nucleus. The excitation energy is determined by the energy of the absorbed particles and 'holes' which are formed as a result of intranuclear cascading. The momentum of the residual nucleus is deduced from momentum conservation, which is applied, in the course of our calculations, at each particle collision.

In the next step, the residual nucleus is described in the framework of statistical equilibrium theory. The calculation of this evaporation stage is carried out by the Monte Carlo method, and in this case the density parameter of the excited state, $a=A/10\ \mathrm{MeV}^{-1}$ [20].

The Coulomb force acting between the projectile and target nucleus is also considered in the model. In fact, in the presence of a Coulomb field the colliding nuclei move along a Coulomb trajectory and not along a straight line. Effectively this corresponds to an increase in the impact parameter and a rotation of all coordinate systems by a particular angle. Both of these quantities are easily found from the study of the classical motion in the Coulomb field.

3. Experiment

Stacks of Br-2 nuclear emulsions were exposed to a 4.1A GeV/c ^{22}Ne beam at the Dubna synchrophasotron. The stacks consisted of 50 or 100 pellicles having dimensions of 20 cm × 10 cm × 600 μm (undeveloped emulsion). The intensity of irradiation was 10^4 particles/cm^2, and the beam diameter was about 1 cm. Along-the-track double scanning was carried out, fast in the forward direction and slow in the backward direction. The scanned beam tracks were further examined by measuring the delta-electron density on each of them to exclude the tracks having charge less than the beam-particle charge.

One-prong events with a secondary-particle track emission angle of less than three degrees and without visible tracks from excitation or distintegration of the target nucleus were excluded due to elastic scattering.

Along a total scanned length of 947.4 m, 9318 inelastic interactions of ^{22}Ne ions with emulsion were recorded, leading to a mean-free path of 10.2±0.1 cm for inelastic interactions. This value and other experimental details have been published by our collaboration in [22–26]. In the measured events, the secondary particles are classified as follows: (i) black particle tracks (b) having a range $L<3$ mm in emulsion which corresponds to a proton kinetic energy of <26 MeV; (ii) grey particle tracks (g) having

relative ionisation $I^*(=I/I_0)>1.4$ and $L>3$ mm which corresponds to a proton kinetic energy of 26–400 MeV, where I is the particle track ionisation and I_0 is the ionisation of a shower track in the narrow forward cone of an opening angle of 3°; (iii) the b and/or g particle tracks are called heavy-ionising-particle tracks (h); (iv) shower particles (s) having $I^*\leqslant 1.4$. Tracks of such a type with an emission angle of <5° were further subjected to rigorous multiple scattering measurement for momentum determination and, consequently, for separating the produced pions and singly charged projectile fragments (protons, deuterons and tritons). The ratio of ^{1}H:^{2}H:^{3}H was found to be 63:27:10 [26]. Further more, the $Z=1$ PF are not included in s particles. (v) The multicharged $Z>2$ PF are subdivided into $Z=2, 3, \ldots, 10$ fragments according to the measured delta-electron and/or gap density. Thus, all particles were adequately divided into PF of $Z=1$–10, target fragments (TF), i.e. h particles, and the generated s particles. The total charge of the PF, $Z^*=\Sigma n_i Z_i$, was calculated in each star, where n_i is the number of fragments of charge Z_i in an event. For each track we obtained from measurements: (*a*) the polar angle θ, i.e. the space angle between the direction of the beam and that of the given track and (*b*) the azimuthal angle Φ, i.e. the angle between the projection of the given track in the plane normal to the beam and the direction perpendicular to the beam in this plane (in an anticlockwise direction).

4. Selection criteria

From the sample of the EXP (4307 interactions) and that of CEM (4976 interactions), we selected events having a PF total charge of $Z^*=10$, i.e. those conserving the charge of the beam nucleus. Thus, 855 events from the experimental sample and 553 events from the simulated interactions were chosen for the present study. Here we study the charge yield distribution for ^{22}Ne projectile fragmentation, the fragment–fragment correlation and the relation between PF and TF. This enables us to distinguish between different theoretical models.

5. Results and discussion

The multiplicity characteristics of the events selected from EXP and CEM are presented in table 1. The values of $\langle n_s\rangle$, $\langle n_g\rangle$ and $\langle n_h\rangle$ in CEM are systematically higher than the corresponding values in EXP. Light and heavy PF are produced in CEM more copiously than in EXP. The PF of medium charge $Z=4$–6 are nearly absent in CEM. This can be explained by the fact that in CEM the light fragments are produced by evaporation and the heavy ones are just residual nuclei of the prefragment systems. Table 1 demonstrates that there is a great difference between CEM and EXP in all average multiplicities of fragments. Table 2 shows the catalogue of 855 selected events, i.e. those having the PF total charge of $Z^*=10$. One can see different channels of fragmentation ordered according to Z_{max}, the charge of the heaviest PF emitted in an interaction. At the beginning one can observe the 'gentle' spallation process in which one or two particles are evaporated from the prefragment nucleus leaving the residual nucleus which cools down, forming a heavy fragment. This process is characterised by low excitation energy and temperature. On the other hand, at the end of the table one can notice a 'violent' process in which the prefragment Ne nucleus has been split into H and He fragments. Figure 1 shows the charge yield curve for fragment production

Table 1. The multiplicity characteristics of the selected events of the total charge of PF, $Z^{tc} = 10$, from EXP and CEM.

		EXP	CEM
$\langle n_s \rangle$		1.30±0.06	1.91±0.09
$\langle n_g \rangle$		0.96±0.06	1.46±0.10
$\langle n_h \rangle$		1.44±0.07	2.34±0.13
$\langle n_{Z=i} \rangle$, $i =$	1	0.99±0.05	1.59±0.11
	2	0.81±0.04	0.36±0.04
	3	0.02±0.01	0±0
	4	0.03±0.01	0.01±0.01
	5	0.04±0.01	0.01±0.01
	6	0.12±0.01	0.02±0.01
	7	0.15±0.01	0.02±0.01
	8	0.23±0.02	0.05±0.01
	9	0.10±0.01	0.12±0.01
	10	0.26±0.02	0.59±0.02

from the ^{22}Ne projectile in the case of collision with emulsion. The distribution has a characteristic U-shaped form. In the region of small Z, the curve decreases, then it rises for large values of Z. The number of target fragments N_h can be used as a measure of the 'violence' of a collision. To demonstrate the correlation between PF and N_h, figure 2 shows the charge distribution of PF for a subclass of events of $N_h = 1$ and $N_h = 4$. In the former case a nearly symmetric U-shaped distribution is obtained which is connected with the 'gentle' low-temperature process. In the latter, the distribution decreases from light to heavier fragments. The class of $N_h = 1$ events cannot be totally attributed to the 'gentle' peripheral collisions. Fragments of small Z in this class of events are mostly the products of 'non-peripheral' collisions between

Table 2. The catalogue of the selected events. Different channels of fragmentation are ordered according to Z_{max}.

Fragmentation channel	Frequency	Fragmentation channel	Frequency
Ne	222	H + Be + B	2
H + F	82	5H + B	4
He + O	142	2B	1
2H + O	49	2H + 2He + Be	9
		4H + He + Be	5
H + He + N	102	3He + Be	4
3H + N	24	H + He + Li + Be	1
2H + He + C	54	3H + 2He + Li	7
2He + C	29	H + 3He + Li	4
4H + C	14	7H + Li	1
H + Li + C	2	H + 3Li	1
Be + C	1	5He	10
		2H + 4He	30
3H + He + B	14	4H + 3He	14
H + 2He + B	13	6H + 2He	5
		8H + He	3

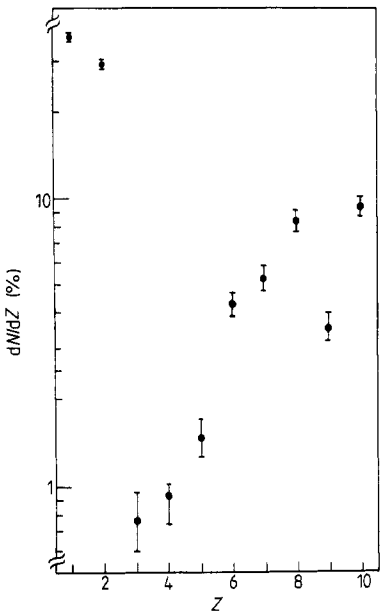

Figure 1. The charge yield distribution of PF from ^{22}Ne fragmentation in emulsion at 4.1*A* GeV/*c*.

^{22}Ne and emulsion. In these events a target nucleon dives into the ^{22}Ne projectile nucleus breaking it into small fragments. The size of the largest fragment which can be formed from the projectile spectator nucleus decreases with decreasing the impact

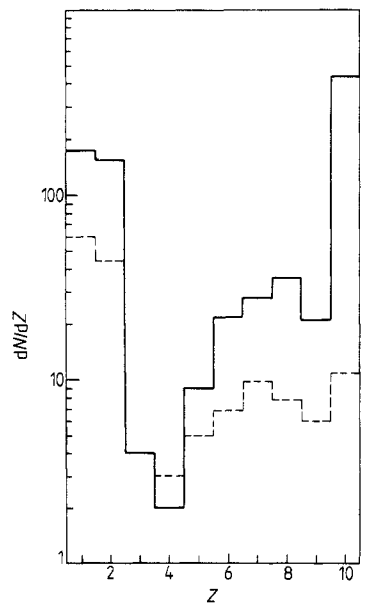

Figure 2. The charge yield distributions of PF from $N_h = 1$ (——) and $N_h = 4$ (– – –) events.

Table 3. The charge distribution of PF as a function of the number of singly charged PF, N_1.

	N_1								
Z	0	1	2	3	4	5	6	7	8
1		207	284	135	132	20	30	7	24
2	262	141	192	28	47		10		3
3		10		7			1	1	
4	5	3	9		5				
5	2	15		14		4			
6	30	2	54		14				
7		102		24					
8	142		49						
9		82							
10	222								

parameter. At $N_h = 1$, fragments of large Z are the evaporation residues of peripheral collisions. Thus, light fragments ($Z = 1$ and 2) are the products of either 'gentle' evaporation or 'violent' multifragmentation.

The degree of 'violence' of a collision can be characterised by the number of singly charged projectile fragments N_1. These fragments are from different sources: direct pick-up during the intranuclear cascade, evaporation and the smallest fragments of the multifragmentation process. In any of these cases the production rate should increase with the degree of 'violence' of the collision or with the excitation energy of

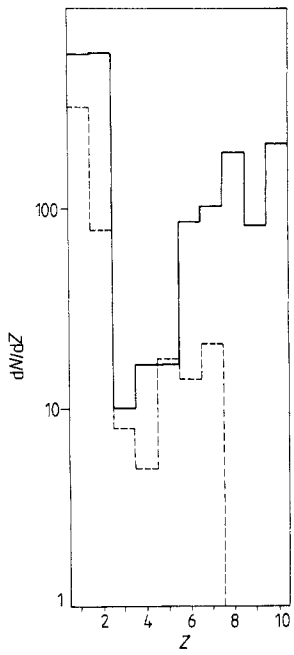

Figure 3. The charge yield distributions of PF from events of the number of singly charged PF, $N_1 \leq 2$ (——) and $N_1 \geq 3$ (– – –).

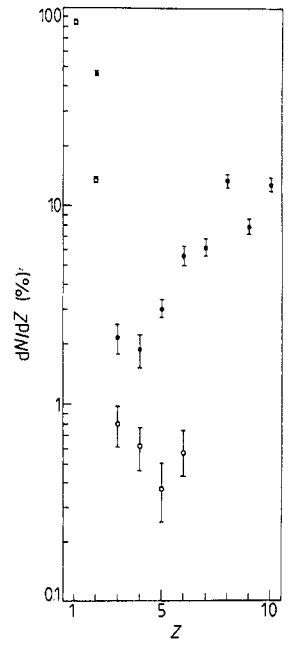

Figure 4. The charge yield distributions of PF from $N_h = 0$ events for $N_1 = 0$ (●) and $N_1 \geq 4$ (○).

Table 4. The dependence of the charge distribution of PF on Z_{max}.

	Z									
Z_{max}	1	2	3	4	5	6	7	8	9	10
2	180	225								
3	33	26	15							
4	39	36	1	19						
5	77	40		2	35					
6	176	112	2	1		100				
7	174	102					126			
8	98	142						191		
9	82								82	
10										222

the emitting source. Table 3 shows the charge distribution of PF as a function of N_1. Figure 3 shows that the charge distribution takes the U-shaped form in the case of $N_1<2$ while it decreases for $N_1>3$. This behaviour is more pronounced in the case of $N_h=0$ events. Figure 4 displays the charge distribution for $N_1=0$ and $N_1>4$ events. The transition from the U-shaped distribution to the monotonically decreasing one is more obvious in this case.

Another measure of the 'violence' of a collision is Z_{max}, the charge of the largest PF emitted in the interaction. Table 4 shows the dependence of the charge distribution of PF on Z_{max}. At large values of Z_{max}, i.e. 'gentle' collisions, the charge distribution of PF

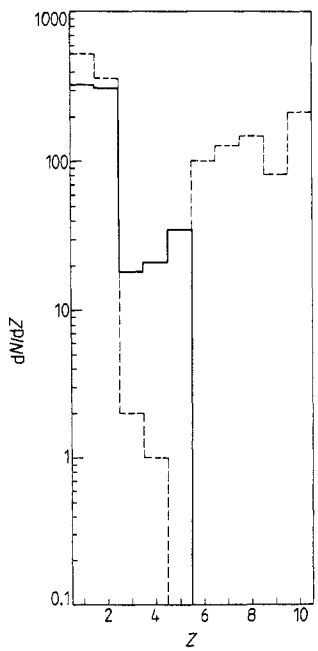

Figure 5. The charge yield distributions of PF from events of $Z_{max}\geq 6$ (– – –) and $Z_{max}<6$ (——).

Table 5. $\langle n_s \rangle$ and $\langle N_h \rangle$ as a function of the number of PF.

$\langle N_{PF} \rangle$	ε^*/A	$\langle n_s \rangle$	$\langle N_h \rangle$
1.51	5	0.64±0.08	1.94±0.18
3.35	7	1.82±0.15	2.69±0.31
5.47	15	2.44±0.38	3.19±0.61
7.62	18	2.81±0.97	4.04±1.38

is a nearly symmetric U-shaped one. At low values of Z_{max}, i.e. 'violent' collisions, the charge distribution is a decreasing function. These features are seen better in figure 5, where the charge distributions are presented for $Z_{max}>6$ and $Z_{max}<6$ events. The analysis of figures 1–5 and tables 1–4 show that the inclusive charge yield distribution of fragments is a superposition of different mechanisms. One can distinguish at least two main classes of mechanism: gentle evaporation and violent multifragmentation. The authors of [17] have interpreted the mass yield curve in the frame of a liquid–gas transition. The present analysis shows that this claim is not conclusive; singly and doubly charged fragments are obviously due to different mechanisms. The violence of the interaction can be measured by the multiplicities of target fragment associated with a projectile fragment. Table 5 presents $\langle n_s \rangle$ and $\langle N_h \rangle$ as a function of the number of PF. The first column represents the average number of PF, the second is the excitation energy per nucleon (in MeV) of the prefragment nucleus calculated according to the statistical model [4], and the third and fourth columns represent the average multiplicities of the associated s and h particles, respectively. The correlation between the multiplicities of PF and TF is clearly seen from table 5. The values of $\langle n_s \rangle$ and $\langle N_h \rangle$ increase systematically with N_{PF}.

The class of events with $N_h = 0$, i.e. those without target fragmentation, have been studied in detail previously for ^{12}C-emulsion collisions at 4.5A GeV/c [27] and at

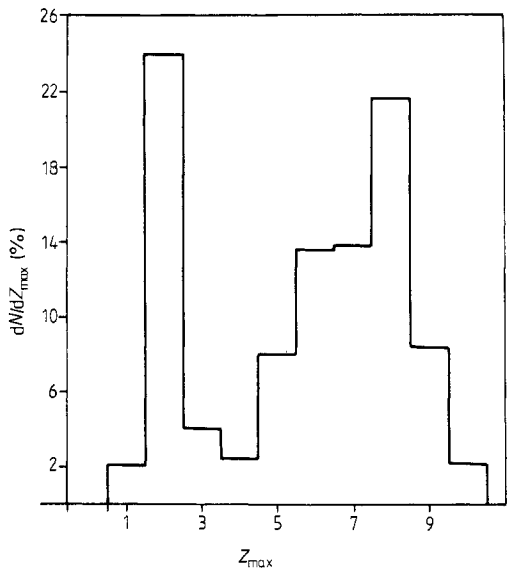

Figure 6. The production frequency of $N_h = 0$ events as a function of Z_{max}.

Table 6. The production frequency in percentage of events in emulsion as a function of Z_{max}, the charge of the heaviest PF in an interaction.

	Z_{max}			
Beam	1	2	3	⩾4
2.1*A* GeV ^{12}C	7±2	59±10	8±3	26±12
4.5*A* GeV ^{12}C	13±4	62±9	15±4	10±3
4.1*A* GeV ^{22}Ne	2±1	24±2	4±1	70±4

2.1*A* GeV/*c* [28]. It is interesting to compare the present data with these results. The production frequency of events in ^{22}Ne–Em collisions as a function of Z_{max} is shown in figure 6 and table 6. It should be noted that the maximum probability is for events having $Z_{max}=2$. In the case of 4.5*A* GeV/*c* ^{12}C–Em collisions [27], the fraction of such events is (62±9)% of all $N_h=0$ events. For 4.1*A* GeV/*c* ^{22}Ne–Em, the corresponding ratio is only (24±2)%. This experimental fact can be interpreted as due to two main reasons. (i) The ^{12}C nucleus is an even–even one of zero total spin, i.e. an α-cluster nucleus. (ii) The main channel of fragmentation is a two-particle one. In the case of ^{22}Ne–Em collisions, Ne→He + O predominates, and both He and O are stable nuclei. The corresponding channel in ^{12}C–Em collisions is ^{12}C→He + Be, but Be is an unstable nucleus which decays directly into two He nuclei. In fact, the percentage of He for ^{12}C–Em collisions is (62±9)%. If this percentage is divided by two, it will be nearly equal to the corresponding value for ^{22}Ne–Em collisions. Table 6 shows that the production frequency of events in emulsion as a function of Z_{max} is independent of energy in the range of a few GeV/*c* per nucleon. It is remarkable that $Z=2$ and $Z=8$ are the first two magic numbers. This explains the peaks observed at these values in figure 6. The results show that the nuclear structure of the prefragment nucleus plays an important role in the fragmentation process. More 'gentle' fragmentations of ^{22}Ne projectile nuclei are the events of $N_h=0$ and $n_s=0$, i.e. those without target fragmentation and generation of shower particles. Table 7 presents a catalogue of the

Table 7. The catalogue of the observed PF in events of $N_h=0$ and $n_s=0$ ordered according to Z_{max}.

Fragmentation channel	Frequency
Ne	3
H + F	18
He + O	56
2H + O	8
H + He + N	10
3H + N	3
2H + He + C	3
2He + C	6
4H + C	1
He + Li + B	1
H + 2He + B	3
3He + Be	2
2H + 2He + Be	1
2H + 4He	1
5He	4

observed PF in the 120 events of $N_h = 0$ and $n_s = 0$ ordered according to Z_{max}. Out of them, the number of single- and double-prong stars is 77 (64.2%). This shows a low excitation energy of the prefragment nucleus, $\varepsilon^*/A \simeq 3$–4 MeV [4].

6. Conclusions

In ^{22}Ne + Em collisions at 4.1A GeV/c, events having the PF total charge Z^* equal to the beam charge have been selected for studying the fragmentation of ^{22}Ne in emulsion.

The inclusive charge distribution of fragments is a superposition of different mechanisms. The heavy fragments ($Z = 8$–10) as well as some of the light ones ($Z = 1, 2$) originate mainly from 'gentle' peripheral collisions. They show a distribution characteristic for evaporation from the compound nucleus. This process is characterisied by low excitation energy. These fragments are associated with a low multiplicity of target tracks. The medium mass fragments as well as the measurable part of $Z = 1$ and 2 fragments are due to non-peripheral 'violent' collisions characterised by associated large multiplicities of the target. The charge distribution of these fragments has a monotonical decreasing shape. Thus, the mechanisms claiming that one hot source at a certain excitation energy explains the inclusive charge distribution conflict with the present analysis.

The presented cascade-evaporation model does not reproduce the average multiplicitiers of projectile and target fragments in the selected class of extreme peripheral collisions of ^{22}Ne + Em at 4.1A GeV/c.

Acknowledgment

AE-N would like to thank the authorities of JINR and Cairo University for supporting him during his stay at Dubna while the present investigation was being carried out.

References

[1] Perfilov N A, Lozhkin O V and Gorichev P A 1960 *Usp. Fiz. Nauk* **70** 3
[2] Hüfner J 1985 *Phys. Rep.* **125** 131
[3] Mishustin I N 1986 *Nucl. Phys.* A **447** 67C
[4] Toneev V D, Schulz H, Gudima K K and Röpke G 1986 *Fiz. E. Ch. Atom. Yad.* **17** 1093
[5] Minich R W *et al* 1982 *Phys. Lett.* **118B** 458
[6] Gross D H E, Satpathy L, Ta-Chung Meng and Satpathy M 1982 *Z. Phys.* A **309** 42
[7] Friedman W A and Lynch W G 1983 *Phys. Rev.* C **28** 950
[8] Randrup J and Koonin S 1981 *Nucl. Phys.* A **356** 223
[9] Das Gupta S and Mekjian A Z 1981 *Phys. Rep.* **72** 131
[10] Bondorf J P, Donangelo R, Mishustin I N, Pethick C J, Schulz H and Sneppen K 1985 *Nucl. Phys.* A **443** 321
[11] Bondorf J P, Donangelo R, Mishustin I N, Pethick C J, Schulz H and Sneppen K 1985 *Nucl. Phys.* A **444** 460
[12] Bondorf J P 1982 *Nucl. Phys.* A **387** 250
[13] Fai G and Randrup J 1982 *Nucl. Phys.* A **381** 557
[14] Aichelin H 1984 *Phys. Rev.* C **30** 107
[15] Campi X 1984 *Phys. Lett.* **142B** 8

[16] Aichelin J and Hüfner J 1984 *Phys. Lett.* **136B** 15
[17] Kaufman S B, Weisfield M W, Steinberg E P, Wilkins B D and Hederson D 1976 *Phys. Rev.* C **14** 1121
[18] Hirosch A S, Bujak A, Finn J E, Gutay L J, Minich R W, Porile N T, Scharenberg R P, Stringfellow B C and Turkot F 1984 *Phys. Rev.* C **29** 508
[19] Barashenkov V S, Zheregi F G and Musulmanbekov Zh Zh 1983 *JINR Preprint, Dubna P 2-83-117*
[20] Barashenkov V S, Il'inov A S, Sobolevskii I M and Toneev V D 1973 *Usp. Fiz. Nauk* **109** 93
[21] Barashenkov V S, Il'inov A S and Toneev V D 1971 *Yad. Fiz.* **13** 743
[22] Bannik B P *et al* 1985 *Z. Phys.* A **321** 249
[23] Bannik B P *et al* 1984 *Zh. Eksp. Teor. Fiz. Pis. Red.* **39** 184 (1984 *JETP Lett.* **39** 219)
[24] Vokalova A *et al* 1984 *JINR Communication, Dubna P1-84-532*
[25] Andreeva N P *et al* 1986 *JINR Preprint, Dubna P1-86-8*
[26] Ameeva B U *et al* 1986 *Izv. Akad. Nauk.* **11** 2703
[27] El-Naghy A 1981 *Z. Phys.* A **302** 261
[28] Heckmann H H, Greiner D E, Lindstrom P J and Shwe H 1978 *Phys. Rev.* C **17** 1735